CHEMISTRY OF MATERIALS

pubs.acs.org/cm Article

Atomistic Mechanism of Passivation of Halide Vacancies in Lead Halide Perovskites by Alkali Ions

Wei Li,* Juan Zhan, Xiaorui Liu, Jianfeng Tang, Wan-Jian Yin,* and Oleg V. Prezhdo*

Cite This: *Chem. Mater.* 2021, 33, 1285−1292 Read Online

ACCESS | Metrics & More | Article Recommendations | Supporting Information

ABSTRACT: Intrinsic defects in perovskite films strongly influence carrier dynamics by introducing nonradiative recombination centers, limiting the performance of perovskite solar cells. Extensive "trail-and-error" experimental efforts have been devoted to defect passivation, requiring fundamental understanding and rational guidance. Using state-of-the-art ab initio quantum dynamics simulations, we demonstrate suppression of nonradiative energy losses in lead halide perovskites with the introduction of monovalent alkali ions. We show that alkali doping of iodine vacancies, the most common defect, eliminates trap states in $MAPbI_3$ and extends charge carrier lifetimes. Negative formation energy is found when alkali cations occupy the B site of the perovskite lattice, identifying the location of the alkali dopants. Iodine vacancy introduces a sub-gap state capable of trapping holes. The state is supported by Pb-p orbitals that interact across the vacancy site. Alkali doping eliminates the trap state by weakening the interaction of Pb-p orbitals across the vacancy and removing extraneous electrons from the conduction band. We demonstrate that the lifetimes grow in the order unpassivated → Li → Na → K-passivated, as rationalized by symmetry breaking, charge localization, and participation of low-frequency phonon modes that lead to changes in electronic structure, nonadiabatic electron−phonon coupling, and quantum coherence time. The atomistic understanding of the various factors contributing to the defect passivation guides development of high-efficiency perovskite devices.

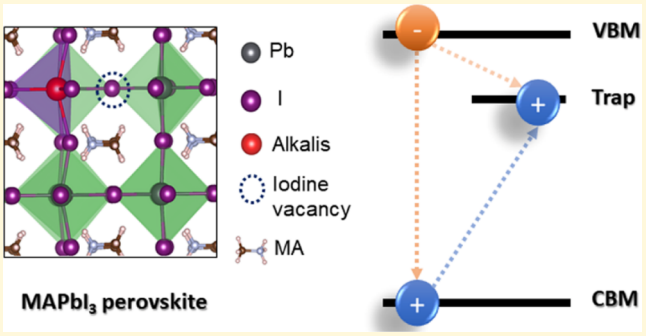

INTRODUCTION

Organic−inorganic hybrid perovskite solar cells (PSCs) have drawn tremendous attention in recent years because of their appealing optoelectronic properties.[1−10] The power conversion efficiency of PSCs has rapidly increased from 3.8 to over 25.2% in just a decade.[11] Several beneficial features of hybrid perovskites, including close to optimal band gaps, large absorption coefficients, small exciton binding energies, low charge recombination rates, and large carrier diffusion lengths, are considered to be the origin of superior performance. Despite significant advances, the certified efficiency of 25.2% is still below the Shockley−Queisser efficiency limit of a single-junction solar cell.[12] Nonradiative recombination of electrons and holes presents the major pathway for charge and energy losses and should be suppressed to further improve the performance of PSCs.

Structural defects are normally presented in solution-processed perovskite films,[13−17] and are capable of introducing sub-gap states, which facilitate nonradiative recombination of photogenerated charge carriers, resulting in low operating voltages and decreased photovoltaic performance. Defects in perovskites have been proposed as the possible cause of other open issues, such as anomalous current−voltage hysteresis and instability against water, oxygen, heat, and ultraviolet light.[15,18−21] Understanding the nature of defects and suggesting the way of removing harmful defects are of particular interest for further device optimization. Theoretical investigations suggest that defects in $MAPbI_3$ perovskite film come mainly from elemental vacancies.[22−29] Several research groups report that halide vacancies in $MAPbI_3$ and related perovskites have low formation energy, aggravate instability, and contribute to nonradiative recombination of charge carriers, motivating researchers to further eliminate these defects.[30,31] Considerable efforts have been devoted to this topic.[20,30,32−36] In particular, compositional engineering via doping provides an effective passivation strategy for defect management in PSCs.

Alkali metal cations, owing to their stability and resistance against oxidation and reduction, have been considered as ideal dopants. Several groups report passivation of intrinsic defects in perovskites by the incorporation of monovalent alkali ions.[37−49] Cao et al. demonstrate that Li-doped perovskites

Received: October 28, 2020
Revised: January 19, 2021
Published: February 1, 2021

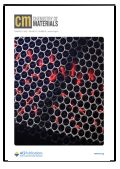

https://dx.doi.org/10.1021/acs.chemmater.0c04188
Chem. Mater. 2021, 33, 1285−1292

exhibit improved electric conductivity.[46] Considerable research studies have also been reported for understanding the Na and K doping in perovskites.[41,44,47,50−55] Li, Na, and K have small ionic radii compared to Cs, which can successfully replace the organic MA cation in the A site of the $MAPbI_3$ perovskite. As a result, when Li, Na, or K occupy the A site, the inorganic Pb−I octahedra collapse due to an unfavorable Goldschmidt tolerance factor. Interestingly, experiments demonstrate that alkali cations do enter the perovskite lattice, especially for the small size Li, as revealed, by X-ray photoemission spectroscopy (XPS) characterization.[56] This indicates that alkali cations may occupy other locations in perovskite instead of the A site. Several teams propose that alkali cations occupy interstitial positions in the $MAPbI_3$ perovskite,[46] whereas others defy this argument.[57] The location of the alkali cations in perovskites and their impact on nonradiative electron−hole recombination remains a topic of debate, calling for detailed theoretical explorations.

In this work, we establish the mechanism of passivation of structural defects in the metal halide perovskites by alkali cations, using a combination of nonadiabatic molecular dynamics (NA-MD) and time-domain density functional theory (TD-DFT). Focusing on iodine vacancy (I_V) in $MAPbI_3$, which is a very common defect in the most popular perovskite, we demonstrate at the atomistic level and in the time domain how vacancy doping by small alkali cations, including Li^+, Na^+, and K^+, eliminates the defect and extends charge carrier lifetimes. The simulations indicate that substitutional occupancy at the B site by alkali cations in the presence of I_V is energetically favored over interstitial occupancy. I_V introduces a trap state near the conduction band (CB) edge owing to the formation of a bonding state formed by p orbitals of Pb atoms around the vacancy. Substitution of a Pb atom near I_V with an alkali metal breaks the Pb-p bonding state, removes the extraneous electron from the CB, and efficiently mitigates the trap state. This finding is consistent with the experimental observation that trap density is reduced upon the addition of alkali cations.[48,50,58] Our state-of-the-art quantum dynamics simulations demonstrate that charge carrier lifetimes grow in the order $I_V \rightarrow Li \rightarrow Na \rightarrow K$. The carrier lifetimes in the K-doped I_V system exceed 100 ns and is a factor of 3 longer than that in the undoped perovskite. Introduction of alkali dopants perturbs system symmetry, pushes electron and hole charge densities away from the vacancy site, and makes the charge densities more localized. As a result, the NA electron−phonon coupling is reduced, and loss of quantum coherence in the electronic subsystem is accelerated, both factors responsible for the lower charge recombination rate. More high-frequency phonons couple to the electronic subsystem upon alkali doping, accelerating decoherence further. The atomistic insights provided in this work uncover the complex, multifactor passivation mechanism of alkali doping in perovskites, and generate valuable guidelines for further optimization of PSCs and related devices.

METHODS

A simulation cell with 96 atoms based on a 2 × 2 × 2 expansion of pseudo-cubic $MAPbI_3$ perovskite is used to represent the pristine system (Figure 1). Defective perovskite, I_V, is created by removing an iodine atom from the pristine system (Figure 1). Alkali-doped systems are constructed by substituting a Pb atom near the vacancy site with a Li, Na, or K atom, as rationalized below. Electronic structure calculations, geometry optimizations, calculations of formation energies, and adiabatic MD are carried out with the Vienna ab initio simulation package (VASP).[59] The Perdew−Burke−Ernzerhof (PBE) functional is adopted to describe electron exchange correlation. A 400 eV kinetic energy cutoff and a 3 × 3 × 3 Γ-centered k-point mesh are used. Atomic positions are relaxed until the forces on all atoms are below 0.02 eV/Å.

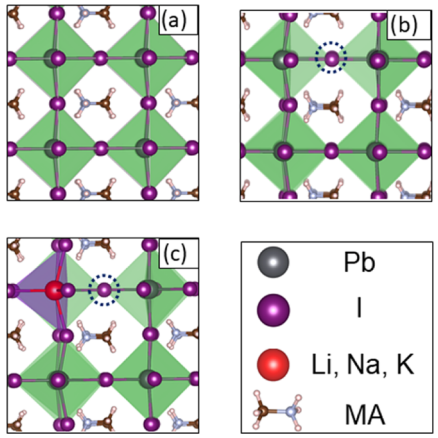

Figure 1. Structures of pristine $MAPbI_3$ (a) and defective $MAPbI_3$ containing an iodine vacancy without (b) and with (c) alkali dopants. The pristine structure is constructed by a 2 × 2 × 2 expansion of bulk $MAPbI_3$ in the cubic phase. The location of the iodine vacancy is denoted by the black dashed circle. The alkali dopants occupy the Pb site, corresponding to the lowest-energy configuration, Li_{Pb} with I_v in Table 1.

The NA-MD simulations are performed using the semiclassical decoherence-induced surface hopping (DISH) method,[60] as implemented in the PYXAID code[61,62] under the classical path approximation (CPA). The CPA allows one to precompute the NA Hamiltonian, and then carry out a large number of stochastic realizations of the surface hopping algorithm, greatly reducing the overall computational cost. The method has been widely used to simulate photoinduced excited-state dynamics in a broad range of systems,[63−71] including perovskites.[72−86] After geometry optimization at 0 K, all systems are heated to 300 K (room temperature) using velocity rescaling. Then, a 3 ps microcanonical ensemble (NVE) MD trajectory at 300 K is obtained and further used for NA electron−phonon coupling calculation. The 3 ps NA Hamiltonians are iterated multiple times to allow averaging over 3000 initial configurations and simulating a long time NA dynamics.

RESULTS AND DISCUSSION

We consider alkali doping of the $MAPbI_3$ perovskite from the thermodynamic perspective, though kinetic factors governing the insertion of alkali species is also an important aspect that needs to be examined in subsequent studies. To determine the most likely location of alkali cations in the defective perovskite, we calculated and compared the energies of Li^+-doping at the interstitial site (Li_i) and the B site (Li_{Pb}). In the latter case, a Pb atom near the vacancy site was substituted by a Li atom, with I_V either present or absent. To avoid the formation of secondary phases, several correlated equations, provided in the Supporting Information, must be satisfied. The formula used to compute the formation energy is presented in the Supporting Information as well. Note that the formation energy of an intrinsic defect is strongly influenced by the chemical potentials (μ) of the constituent species. We use the chemical potentials of the atomic components, μ(MA), μ(Pb), and μ(I), as the reference, as has been adopted in the community.[22] In particular, we do not use the PbI_2 and MAI precursors as the reference because we need atomic chemical potentials to define

https://dx.doi.org/10.1021/acs.chemmater.0c04188
Chem. Mater. 2021, 33, 1285−1292

the energy of substitution of Pb with Li. We choose representative values of the chemical potentials within a thermodynamically stable range of perovskite growth, with $\mu(I) = -1.12$ eV and $\mu(Li) = -1.4$ eV for I-rich conditions and $\mu(Pb) = -2.24$ eV and $\mu(Li) = -2.53$ eV for Pb-rich conditions. The computed formation energies of the considered defects at neutral charge are listed in Table 1.

Table 1. Formation Energy (eV) of Neutral Li_{Pb} and Li_i Defects under Pb-Rich and I-Rich Conditions

	without I_V		with I_V	
	Li_{Pb}	Li_i	Li_{Pb}	Li_i
Pb-rich	0.39	1.9	−1.76	2.16
I-rich	1.51	0.82	−0.65	1.03

The formation energies of Li_{Pb} in the presence of I_V are negative for both I-rich and Pb-rich conditions, indicating that Li is able to spontaneously occupy the Pb site in this configuration. The concentration of Li_{Pb} can be controlled experimentally by tuning the chemical potential of Li. Other doping scenarios, including Li_i in the presence of I_V and Li_{Pb} in pristine perovskite, give much higher formation energies. The low formation energy of Li_{Pb} in I_V can be rationalized by two factors. First, when Li substitutes Pb, Li_{Pb} is an acceptor-like defect, and it is well compensated by the donor-like I_V. Hence, the formation of Li_{Pb} in the presence of an iodine vacancy is more favorable than the formation of Li_i. Therefore, Li-doped $MAPbI_3$ should be in the iodine vacancy structure and in the octahedral configuration. Second, iodine vacancies decrease the steric hindrance for Li to penetrate into the perovskite lattice. The calculations indicate that the occupancy of Li at the B site of I_V is most thermodynamically stable. Note that the prior work also showed that the introduced Li can occupy the B site of ABX_3-type oxides to form the octahedral configuration.[53] We also find a similar trend for the formation energy of the Na- and K-doped systems (not shown herein). Therefore, we focus on this type of occupancy for all considered alkali dopants in the NA-MD calculations.

The evolution of the distances between the alkali cations and the two nearby iodine atoms during the NVE-MD trajectories is shown in Figure 2. The Na−I and K−I bond lengths fluctuate by a few tenths of an Angstrom around their equilibrium values. The Li−I bonds fluctuate more significantly because Li^+ is small and light and can move within the available space. The data in Figure 2 suggest that Li^+ binds to one or the other iodine. The inorganic network of the Pb−I octahedra is persevered during the thermal fluctuations.

The projected densities of states (pDOSs) $MAPbI_3$ containing I_V before and after Li^+-doping are shown in Figure 3. The insets present the charge densities of the band edge states. The pDOS of the pristine perovskite, and the pDOS of the Na^+- and K^+-doped perovskites are shown in the Supporting Information. The computed band gap of the pristine perovskite is about 1.7 eV, in agreement with the experiment and other theory works.[87−90] The I_V systems before and after alkali doping have the band gaps comparable to that of pristine perovskite. For all systems, the valence band maximum (VBM) arises from the antibonding coupling of the Pb-s and I-p orbitals, whereas the CB minimum (CBM) is primarily due to the antibonding coupling between Pb-p and I-p orbitals. The alkali cations have almost no contribution to the band edge states. The iodine vacancy introduces a shallow

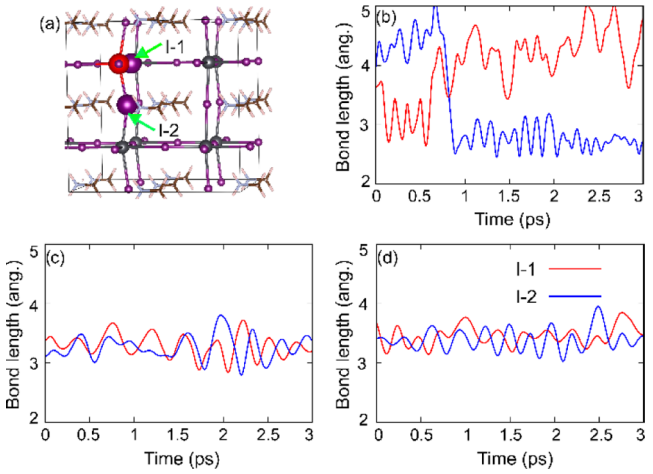

Figure 2. Fluctuations of distances between the dopant and nearest iodine atoms along the MD trajectories at room temperature. Panel (a) specifies the location of the two iodines. Panels (b), (c), and (d) show distances between each of the two iodines and Li, Na, or K, respectively. Because Li is small, it moves significantly and hops between different iodine atoms. The larger-sized Na and K can bond to both iodines simultaneously.

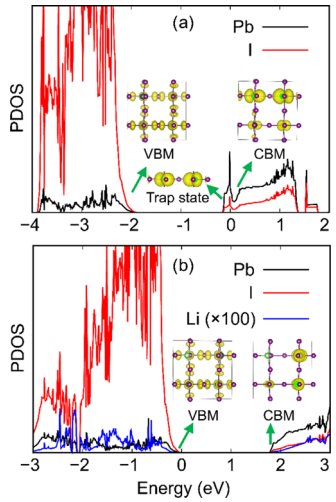

Figure 3. Projected density of states (pDOS) for defective $MAPbI_3$ containing an iodine vacancy without (a) and with (b) Li doping. The insets show charge densities of the band edge and trap states, with the organic cations removed to guide the eye. pDOS for pristine $MAPbI_3$, and the Na^+- and K^+-doped systems are provided in the Supporting Information. Iodine vacancy creates a shallow trap state close to the CBM. The trap state disappears in the alkali-doped perovskite due to the breaking of the Pb *pp* bonding state.

trap state that derives from the CB. The trap state is formed by *p* orbitals of the nearby Pb cations that now contain an unsaturated chemical bond. The trap state is located below the Fermi level and is populated with electrons, acting as a hole trap. Holes generated in the valence band (VB) upon photoexcitation can be trapped by this state prior to their recombination with CB electrons.

It has been shown that the defect level of halide vacancy is intrinsically dynamic.[91] Fluctuation in the defect-level energy depends on the distance between the neighboring Pb−Pb across the halide vacancy. Shorter Pb−Pb distances across the vacancy favor stronger *pp* orbital coupling between the nearby Pb atoms, making the defect level deeper. One may expect that

https://dx.doi.org/10.1021/acs.chemmater.0c04188
Chem. Mater. 2021, 33, 1285−1292

reducing the strength of *pp* coupling can mitigate the unwanted defect level. Figures 3b and S1 show that the trap state disappears in the alkali-doped perovskite. This is because the alkali cation replaces a Pb atom near the vacancy and correspondingly breaks the *pp* bonding state. The destruction of the *pp* bonding state is particularly important when the iodine vacancy is negatively charged because the negative charge attracts the Pb cations, resulting in the formation of a Pb−Pb dimer with a deep defect level.[29] The elimination of the defect level by alkali passivation is expected to strongly influence the charge carrier dynamics. In addition to the defect-level energy, alkali doping also influences the charge density distributions. As shown in Figure 3, the VBM and CBM in the alkali-doped perovskite are more localized. The wavefunction localization can decrease the overlap of electron and hole wavefunctions and weaken the NA electron−phonon coupling. It can also reduce the correlation between electron and hole, and accelerate the decoherence process.

To gain insights into the phonon modes participating in the nonradiative electron−phonon relaxation, we calculate the spectral density obtained by Fourier transform of the autocorrelation function of the energy gap fluctuation (Figure 4). The intensity characterizes the strength of the electron−

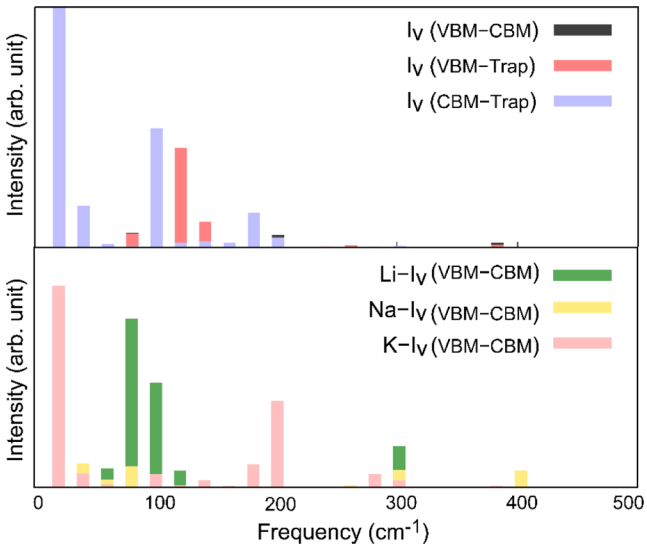

Figure 4. Fourier transforms of autocorrelation functions for the energy gaps between the key states. The top panel refers to the iodine vacancy, while the bottom panel shows data for the Li^+-, Na^+-, and K^+-passivated vacancies. Alkali doping introduces high-frequency phonon modes, facilitating rapid loss of quantum coherence.

phonon coupling for each mode. The spectra are dominated by sub-200 cm^{-1} frequencies, which can be assigned to vibrations of the Pb−I inorganic lattice, in agreement with the Raman characterization[92] and the previous simulations.[83] Involvement of low-frequency phonon modes in the charge recombination process is not surprising, since band edge states are supported by heavy Pb and I atoms. Some high-frequency modes with lower intensity are present in the 300−400 cm^{-1} range, associated with torsional motions of MA cations. This observation reflects the indirect influence of MA cations on the electron−phonon relaxation. MA cations carry no contributions to the band edge states but may influence vibrational motions of the inorganic Pb−I lattice via electrostatic interaction and dipole orientation, as well as by steric repulsion.[93] Higher frequencies are more evident in the alkali-doped systems since alkali atoms are also light compared to Pb and I. Overall, electrons and holes couple to a wider range of modes in the alkali-doped systems. Participation of a broader spectrum of vibrations contributes to faster loss of quantum coherence.

We compute the decoherence time as the pure-dephasing time of the optical response theory. The pure-dephasing time can be accessed experimentally either directly or as the inverse of the homogeneous optical linewidth. The second-order cumulant approximation to the optical response function is employed.[94−98] The data are listed in Table 2. The quantum

Table 2. Band Gap (E_g, eV), Absolute NA Coupling (|NAC|, meV), Pure-Dephasing Time (fs), and Rate Constant (ns^{-1}) for VBM−CBM (VC), VBM−Trap (VT), and CBM−Trap (CT) Transitions in the Defective and Alkali-Doped Perovskites

	I_V			Li−I_V	Na−I_V	K−I_V
	VC	VT	CT	VC	VC	VC
E_g	1.8	1.7	0.1	1.77	1.8	1.81
|NAC|	0.50	0.30	2.1	0.43	0.39	0.31
dephasing	11.2	7.9	20.7	10.4	9.7	6.1
rate	0.022	0.017	18.84	0.015	0.012	0.0097

Zeno effect illustrates the strong influence of quantum coherence within the electronic subsystem on the electron−phonon relaxation.[99] When the quantum transition is much slower than coherence loss, faster decoherence makes the transition slower, extending charge carrier lifetimes. As shown in Table 2, decoherence between all pairs of states is very fast and proceeds on a ∼10 fs time scale. The CBM → trap transition in the I_V system constitutes an exception. The corresponding decoherence time is relatively long, 20.7 fs, because the CBM and the trap state have similar chemical compositions and because the CBM−trap gap is small. Generally, smaller gaps have smaller fluctuations, and smaller gap fluctuation results in longer coherence.[94] Decoherence is faster in the alkali-doped perovskites than in the undoped system because the VBM and CBM charge densities are more localized. The decoherence time increases in the order K → Na → Li → I_V. Interestingly, even though the Li atom is much lighter than Na and K and moves faster, the speed of the alkali atom has little influence on the decoherence time. Rapid decoherence slows down the nonradiative recombination of charge carriers, as manifested by the quantum Zeno effect.[99]

Figure 5 presents the evolution of the excited-state populations for the undoped and doped $MAPbI_3$ containing I_V. The plots are constructed by solving coupled kinetic equations with the state-to-state transition rates reported in Table 2. The recombination lifetimes, shown in Figure 5, are obtained by fitting the curves with exponential, $P(t) = \exp(-t/\tau)$. The simulation results show that alkali doping has a strong influence on the nonradiative electron−hole recombination. The I_V system has a charge recombination time of 26 ns. The previous work[29] investigated the nonradiative charge recombination in pristine $MAPbI_3$. The reported excited-state lifetime was 150 ns, indicating that the iodine vacancy accelerates charge carrier losses. The charge recombination time increases upon alkali doping in the following order, I_V → Li → Na → K. The iodine vacancy system shows the fastest relaxation since the trap state provides an additional relaxation channel. Alkali

https://dx.doi.org/10.1021/acs.chemmater.0c04188
Chem. Mater. 2021, 33, 1285−1292

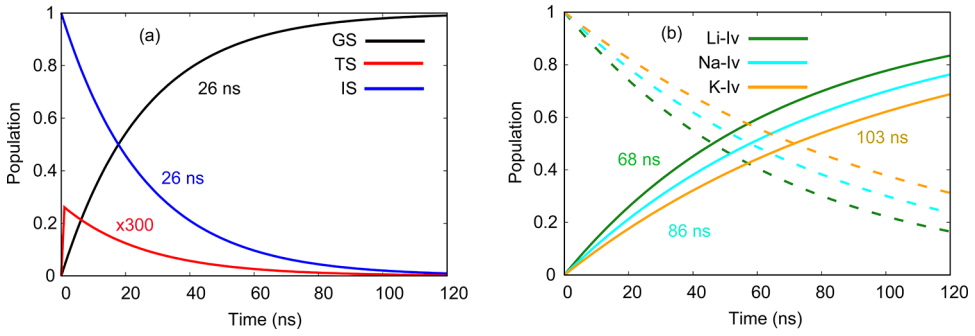

Figure 5. Evolution of the excite-state populations in $MAPbI_3$ containing iodine vacancy (a) and the vacancy passivated with different alkali cations (b). GS, TS, and IS in (a) denote the ground state, trap state, and initial state, respectively. Alkali doping eliminates the trap state and delays charge recombination.

doping eliminates the trap state and delays charge recombination. Generally, differences in the charge recombination rates can be explained by an interplay between NA coupling, electronic band gap, and pure-dephasing time. The VBM−CBM gaps are similar in all systems. The smaller NA coupling and faster decoherence rationalize the slower recombination in the alkali-doped perovskites. Slower charge recombination is beneficial for solar cell performance since it maintains long-lived charge carriers and minimizes charge and energy losses.

CONCLUSIONS

In summary, we have established the mechanism of passivation of the most common defect in PSCs by alkali doping and characterized the factors responsible for enhanced charge carrier lifetimes in alkali-doped perovskites. The alkali cations can occupy the B site of the perovskite lattice, as rationalized by the lower formation energy of the substitutional occupancy with respect to the interstitial occupancy. An iodine vacancy introduces a shallow defect level inside the band gap. The level is populated with electrons and acts as a hole trap. Electronic structure analysis indicates that the trap originates from the bonding state formed by Pb-p orbitals across the vacancy site. When a Pb atom near the vacancy site is replaced with an alkali atom, the Pb *pp* coupling across the vacancy vanishes, extraneous electrons are removed from the CB, and the trap state is mitigated. By passivating the iodine vacancy defect in the $MAPbI_3$ perovskite, alkali doping slows down the charge recombination process. This is demonstrated by the time-domain atomistic quantum dynamics simulations performed with the state-of-the-art methodology developed in our group and combining TD-DFT and NA-MD. In addition to the elimination of the trap state, two more factors contribute to the enhanced charge carrier lifetimes. First, alkali metal dopants perturb system symmetry and make charge densities of the band edge states more localized. This reduces the overlap of electron and hole wavefunctions, and decreases the NA electron−phonon coupling matrix elements. Second, coherence loss in the electronic subsystems is accelerated upon alkali cation doping owing to the more localized charge densities and a broader range of participating phonon modes, in particular those with higher frequencies. The simulations generate important insights into the mechanisms of defect passivation in perovskites and provide theory guidelines for the enhancement of photon conversion efficiencies in PSCs and related devices.

ASSOCIATED CONTENT

Supporting Information

The Supporting Information is available free of charge at https://pubs.acs.org/doi/10.1021/acs.chemmater.0c04188.

Equations for defect formation energies and densities of states of pristine $MAPbI_3$ and $MAPbI_3$ containing iodine vacancy doped by Li^+ and K^+ (PDF)

AUTHOR INFORMATION

Corresponding Authors

Wei Li − *School of Chemistry and Materials Science, Hunan Agricultural University, Changsha 410128, People's Republic of China;* orcid.org/0000-0002-9999-5081; Email: weili@hunau.edu.cn

Wan-Jian Yin − *College of Energy, Soochow Institute for Energy and Materials InnovationS (SIEMIS), Soochow University, Suzhou 215006, People's Republic of China;* orcid.org/0000-0003-0932-2789; Email: wjyin@suda.edu.cn

Oleg V. Prezhdo − *Department of Chemistry, University of Southern California, Los Angeles, California 90089, United States;* orcid.org/0000-0002-5140-7500; Email: prezhdo@usc.edu

Authors

Juan Zhan − *School of Chemistry and Materials Science, Hunan Agricultural University, Changsha 410128, People's Republic of China*

Xiaorui Liu − *School of Chemistry and Chemical Engineering, Southwest University, Chongqing 400715, People's Republic of China*

Jianfeng Tang − *School of Chemistry and Materials Science, Hunan Agricultural University, Changsha 410128, People's Republic of China*

Complete contact information is available at: https://pubs.acs.org/10.1021/acs.chemmater.0c04188

Notes

The authors declare no competing financial interest.

ACKNOWLEDGMENTS

W.L. acknowledges the National Natural Science Foundation of China (Grant No. 21903023) and that Natural Science Foundation of Hunan Province (Grant No. 2020JJ5225). X.L. acknowledges the National Natural Science Foundation of China (Grant No. 21803043). J.T. acknowledges the Double

First-Class Construction Project of Hunan Agricultural University (No. SYL2019063) and the Natural Science Foundation of Hunan Province (Grant No. 2020JJ4375). W.-J.Y. acknowledges funding from the National Natural Science Foundation of China (Grant Nos. 11674237 and 11974257) and the Priority Academic Program Development of Jiangsu Higher Education Institutions (PAPD). O.V.P. acknowledges funding from the U.S. National Science Foundation (Grant No. CHE-1900510).

REFERENCES

(1) Luo, D.; Su, R.; Zhang, W.; Gong, Q.; Zhu, R. Minimizing Non-Radiative Recombination Losses in Perovskite Solar Cells. *Nat. Rev. Mater.* **2020**, *5*, 44−60.

(2) Tremblay, M.-H.; Bacsa, J.; Zhao, B.; Pulvirenti, F.; Barlow, S.; Marder, S. R. Structures of $(4\text{-Y-}C_6H_4CH_2NH_3)_2PbI_4$ {Y = H, F, Cl, Br, I}: Tuning of Hybrid Organic Inorganic Perovskite Structures from Ruddlesden−Popper to Dion−Jacobson Limits. *Chem. Mater.* **2019**, *31*, 6145−6153.

(3) Chen, Y.; Zhou, H. Defects Chemistry in High-Efficiency and Stable Perovskite Solar Cells. *J. Appl. Phys.* **2020**, *128*, No. 060903.

(4) Bernard, G. M.; Wasylishen, R. E.; Ratcliffe, C. I.; Terskikh, V.; Wu, Q.; Buriak, J. M.; Hauger, T. Methylammonium Cation Dynamics in Methylammonium Lead Halide Perovskites: A Solid-State NMR Perspective. *J. Phys. Chem. A* **2018**, *122*, 1560−1573.

(5) Niu, S.; Sarkar, D.; Williams, K.; Zhou, Y.; Li, Y.; Bianco, E.; Huyan, H.; Cronin, S. B.; McConney, M. E.; Haiges, R.; Jaramillo, R.; Singh, D. J.; Tisdale, W. A.; Kapadia, R.; Ravichandran, J. Optimal Bandgap in a 2D Ruddlesden−Popper Perovskite Chalcogenide for Single-Junction Solar Cells. *Chem. Mater.* **2018**, *30*, 4882−4886.

(6) Yoon, S. J.; Draguta, S.; Manser, J. S.; Sharia, O.; Schneider, W. F.; Kuno, M.; Kamat, P. V. Tracking Iodide and Bromide Ion Segregation in Mixed Halide Lead Perovskites during Photo-irradiation. *ACS Energy Lett.* **2016**, *1*, 290−296.

(7) Brennan, M. C.; Draguta, S.; Kamat, P. V.; Kuno, M. Light-Induced Anion Phase Segregation in Mixed Halide Perovskites. *ACS Energy Lett.* **2018**, *3*, 204−213.

(8) Yin, J.; Maity, P.; Naphade, R.; Cheng, B.; He, J.-H.; Bakr, O. M.; Brédas, J.-L.; Mohammed, O. F. Tuning Hot Carrier Cooling Dynamics by Dielectric Confinement in Two-Dimensional Hybrid Perovskite Crystals. *ACS Nano* **2019**, *13*, 12621−12629.

(9) Quarti, C.; De Angelis, F.; Beljonne, D. Influence of Surface Termination on the Energy Level Alignment at the CH_3 NH_3 PbI_3 Perovskite/C60 Interface. *Chem. Mater.* **2017**, *29*, 958−968.

(10) Yin, J.; Yang, H.; Song, K.; El-Zohry, A. M.; Han, Y.; Bakr, O. M.; Brédas, J.-L.; Mohammed, O. F. Point Defects and Green Emission in Zero-Dimensional Perovskites. *J. Phys. Chem. Lett.* **2018**, *9*, 5490−5495.

(11) Jeon, N. J.; Na, H.; Jung, E. H.; Yang, T.-Y.; Lee, Y. G.; Kim, G.; Shin, H.-W.; Seok, S. I.; Lee, J.; Seo, J. A Fluorene-Terminated Hole-Transporting Material for Highly Efficient and Stable Perovskite Solar Cells. *Nat. Energy* **2018**, *3*, 682−689.

(12) Shockley, W.; Queisser, H. J. Detailed Balance Limit of Efficiency of P-n Junction Solar Cells. *J. Appl. Phys.* **1961**, *32*, 510−519.

(13) Meggiolaro, D.; De Angelis, F. First-Principles Modeling of Defects in Lead-Halide Perovskites: Best Practices and Open Issues. *ACS Energy Lett.* **2018**, *3*, 2206−2222.

(14) Meggiolaro, D.; Mosconi, E.; De Angelis, F. Formation of Surface Defects Dominates Ion Migration in Lead-Halide Perovskites. *ACS Energy Lett.* **2019**, *4*, 779−785.

(15) Ball, J. M.; Petrozza, A. Defects in Perovskite-Halides and Their Effects in Solar Cells. *Nat. Energy* **2016**, *1*, No. 16149.

(16) Wu, X.; Trinh, M. T.; Niesner, D.; Zhu, H.; Norman, Z.; Owen, J. S.; Yaffe, O.; Kudisch, B. J.; Zhu, X.-Y. Trap States in Lead Iodide Perovskites. *J. Am. Chem. Soc.* **2015**, *137*, 2089−2096.

(17) Chen, X.; Cheng, S.; Xiao, L.; Sun, H. Identifying, Understanding and Controlling Defects and Traps in Halide Perovskites for Optoelectronic Devices: A Review. *J. Phys. D: Appl. Phys.* **2020**, *53*, No. 373001.

(18) Huang, J.; Yuan, Y.; Shao, Y.; Yan, Y. Understanding the Physical Properties of Hybrid Perovskites for Photovoltaic Applications. *Nat. Rev. Mater.* **2017**, *2*, No. 17042.

(19) Wang, F.; Bai, S.; Tress, W.; Hagfeldt, A.; Gao, F. Defects Engineering for High-Performance Perovskite Solar Cells. *npj Flexible Electron.* **2018**, *2*, No. 22.

(20) Rudd, P. N.; Huang, J. Metal Ions in Halide Perovskite Materials and Devices. *Trends Chem.* **2019**, *1*, 394−409.

(21) Jin, H.; Debroye, E.; Keshavarz, M.; G. Scheblykin, I.; J. Roeffaers, M. B.; Hofkens, J.; Steele, J. A. It's a Trap! On the Nature of Localised States and Charge Trapping in Lead Halide Perovskites. *Mater. Horiz.* **2020**, *7*, 397−410.

(22) Yin, W.-J.; Shi, T.; Yan, Y. Unusual Defect Physics in $CH_3NH_3PbI_3$ Perovskite Solar Cell Absorber. *Appl. Phys. Lett.* **2014**, *104*, No. 063903.

(23) Azpiroz, J. M.; Mosconi, E.; Bisquert, J.; Angelis, F. D. Defect Migration in Methylammonium Lead Iodide and Its Role in Perovskite Solar Cell Operation. *Energy Environ. Sci.* **2015**, *8*, 2118−2127.

(24) Buin, A.; Comin, R.; Xu, J.; Ip, A. H.; Sargent, E. H. Halide-Dependent Electronic Structure of Organolead Perovskite Materials. *Chem. Mater.* **2015**, *27*, 4405−4412.

(25) Du, M.-H. Density Functional Calculations of Native Defects in $CH_3NH_3PbI_3$: Effects of Spin−Orbit Coupling and Self-Interaction Error. *J. Phys. Chem. Lett.* **2015**, *6*, 1461−1466.

(26) Walsh, A.; Scanlon, D. O.; Chen, S.; Gong, X. G.; Wei, S.-H. Self-Regulation Mechanism for Charged Point Defects in Hybrid Halide Perovskites. *Angew. Chem., Int. Ed.* **2015**, *54*, 1791−1794.

(27) Frost, J. M.; Walsh, A. What Is Moving in Hybrid Halide Perovskite Solar Cells? *Acc. Chem. Res.* **2016**, *49*, 528−535.

(28) Yang, J.-H.; Yin, W.-J.; Park, J.-S.; Wei, S.-H. Fast Self-Diffusion of Ions in $CH_3NH_3PbI_3$: The Interstiticaly Mechanism versus Vacancy-Assisted Mechanism. *J. Mater. Chem. A* **2016**, *4*, 13105−13112.

(29) Li, W.; Sun, Y.-Y.; Li, L.; Zhou, Z.; Tang, J.; Prezhdo, O. V. Control of Charge Recombination in Perovskites by Oxidation State of Halide Vacancy. *J. Am. Chem. Soc.* **2018**, *140*, 15753−15763.

(30) Tan, S.; Yavuz, I.; Weber, M. H.; Huang, T.; Chen, C.-H.; Wang, R.; Wang, H.-C.; Ko, J. H.; Nuryyeva, S.; Xue, J.; Zhao, Y.; Wei, K.-H.; Lee, J.-W.; Yang, Y. Shallow Iodine Defects Accelerate the Degradation of α-Phase Formamidinium Perovskite. *Joule* **2020**, *4*, 2426−2442.

(31) Zhu, X.; Lee, J.; Lu, W. D. Iodine Vacancy Redistribution in Organic−Inorganic Halide Perovskite Films and Resistive Switching Effects. *Adv. Mater.* **2017**, *29*, No. 1700527.

(32) Akin, S.; Arora, N.; Zakeeruddin, S. M.; Grätzel, M.; Friend, R. H.; Dar, M. I. New Strategies for Defect Passivation in High-Efficiency Perovskite Solar Cells. *Adv. Energy Mater.* **2020**, *10*, No. 1903090.

(33) Gao, F.; Zhao, Y.; Zhang, X.; You, J. Recent Progresses on Defect Passivation toward Efficient Perovskite Solar Cells. *Adv. Energy Mater.* **2020**, *10*, No. 1902650.

(34) Aydin, E.; Bastiani, M. D.; Wolf, S. D. Defect and Contact Passivation for Perovskite Solar Cells. *Adv. Mater.* **2019**, *31*, No. 1900428.

(35) Ghosh, D.; Smith, A. R.; Walker, A. B.; Islam, M. S. Mixed A-Cation Perovskites for Solar Cells: Atomic-Scale Insights Into Structural Distortion, Hydrogen Bonding, and Electronic Properties. *Chem. Mater.* **2018**, *30*, 5194−5204.

(36) He, Y.; Galli, G. Instability and Efficiency of Mixed Halide Perovskites $CH_3NH_3AI_{3-X}Cl_x$ (A = Pb and Sn): A First-Principles, Computational Study. *Chem. Mater.* **2017**, *29*, 682−689.

(37) Phung, N.; Félix, R.; Meggiolaro, D.; Al-Ashouri, A.; Sousa e Silva, G.; Hartmann, C.; Hidalgo, J.; Köbler, H.; Mosconi, E.; Lai, B.; Gunder, R.; Li, M.; Wang, K.-L.; Wang, Z.-K.; Nie, K.; Handick, E.; Wilks, R. G.; Marquez, J. A.; Rech, B.; Unold, T.; Correa-Baena, J.-P.; Albrecht, S.; De Angelis, F.; Bär, M.; Abate, A. The Doping

Mechanism of Halide Perovskite Unveiled by Alkaline Earth Metals. *J. Am. Chem. Soc.* **2020**, *142*, 2364−2374.
(38) Liu, C.; Sun, J.; Tan, W. L.; Lu, J.; Gengenbach, T. R.; McNeill, C. R.; Ge, Z.; Cheng, Y.-B.; Bach, U. Alkali Cation Doping for Improving the Structural Stability of 2D Perovskite in 3D/2D PSCs. *Nano Lett.* **2020**, *20*, 1240−1251.
(39) Zhou, S.; Ma, Y.; Zhou, G.; Xu, X.; Qin, M.; Li, Y.; Hsu, Y.-J.; Hu, H.; Li, G.; Zhao, N.; Xu, J.; Lu, X. Ag-Doped Halide Perovskite Nanocrystals for Tunable Band Structure and Efficient Charge Transport. *ACS Energy Lett.* **2019**, *4*, 534−541.
(40) Yang, Y.; Wu, L.; Hao, X.; Tang, Z.; Lai, H.; Zhang, J.; Wang, W.; Feng, L. Beneficial Effects of Potassium Iodide Incorporation on Grain Boundaries and Interfaces of Perovskite Solar Cells. *RSC Adv.* **2019**, *9*, 28561−28568.
(41) Xiang, S.; Li, W.; Wei, Y.; Liu, J.; Liu, H.; Zhu, L.; Yang, S.; Chen, H. Natrium Doping Pushes the Efficiency of Carbon-Based $CsPbI_3$ Perovskite Solar Cells to 10.7%. *iScience* **2019**, *15*, 156−164.
(42) Chen, W.; Zhou, Y.; Chen, G.; Wu, Y.; Tu, B.; Liu, F.-Z.; Huang, L.; Ng, A. M. C.; Djurišić, A. B.; He, Z. Alkali Chlorides for the Suppression of the Interfacial Recombination in Inverted Planar Perovskite Solar Cells. *Adv. Energy Mater.* **2019**, *9*, No. 1803872.
(43) Zhao, W.; Yao, Z.; Yu, F.; Yang, D.; Liu, S. F. Alkali Metal Doping for Improved $CH_3NH_3PbI_3$ Perovskite Solar Cells. *Adv. Sci.* **2018**, *5*, No. 1700131.
(44) Tang, Z.; Uchida, S.; Bessho, T.; Kinoshita, T.; Wang, H.; Awai, F.; Jono, R.; Maitani, M. M.; Nakazaki, J.; Kubo, T.; Segawa, H. Modulations of Various Alkali Metal Cations on Organometal Halide Perovskites and Their Influence on Photovoltaic Performance. *Nano Energy* **2018**, *45*, 184−192.
(45) Fang, Z.; He, H.; Gan, L.; Li, J.; Ye, Z. Understanding the Role of Lithium Doping in Reducing Nonradiative Loss in Lead Halide Perovskites. *Adv. Sci.* **2018**, *5*, No. 1800736.
(46) Cao, J.; Tao, S. X.; Bobbert, P. A.; Wong, C.-P.; Zhao, N. Interstitial Occupancy by Extrinsic Alkali Cations in Perovskites and Its Impact on Ion Migration. *Adv. Mater.* **2018**, *30*, No. 1707350.
(47) Abdi-Jalebi, M.; Pazoki, M.; Philippe, B.; Dar, M. I.; Alsari, M.; Sadhanala, A.; Divitini, G.; Imani, R.; Lilliu, S.; Kullgren, J.; Rensmo, H.; Grätzel, M.; Friend, R. H. Dedoping of Lead Halide Perovskites Incorporating Monovalent Cations. *ACS Nano* **2018**, *12*, 7301−7311.
(48) Abdi-Jalebi, M.; Andaji-Garmaroudi, Z.; Cacovich, S.; Stavrakas, C.; Philippe, B.; Richter, J. M.; Alsari, M.; Booker, E. P.; Hutter, E. M.; Pearson, A. J.; Lilliu, S.; Savenije, T. J.; Rensmo, H.; Divitini, G.; Ducati, C.; Friend, R. H.; Stranks, S. D. Maximizing and Stabilizing Luminescence from Halide Perovskites with Potassium Passivation. *Nature* **2018**, *555*, 497−501.
(49) Muzammal uz Zaman, M.; Imran, M.; Saleem, A.; Kamboh, A. H.; Arshad, M.; Khan, N. A.; Akhter, P. Potassium Doped Methylammonium Lead Iodide ($MAPbI_3$) Thin Films as a Potential Absorber for Perovskite Solar Cells; Structural, Morphological, Electronic and Optoelectric Properties. *Phys. B: Condens. Matter* **2017**, *522*, 57−65.
(50) Zheng, F.; Chen, W.; Bu, T.; Ghiggino, K. P.; Huang, F.; Cheng, Y.; Tapping, P.; Kee, T. W.; Jia, B.; Wen, X. Triggering the Passivation Effect of Potassium Doping in Mixed-Cation Mixed-Halide Perovskite by Light Illumination. *Adv. Energy Mater.* **2019**, *9*, No. 1901016.
(51) Li, C.; Wang, A.; Xie, L.; Deng, X.; Liao, K.; Yang, J.; Li, T.; Hao, F. Emerging Alkali Metal Ion (Li^+, Na^+, K^+ and Rb^+) Doped Perovskite Films for Efficient Solar Cells: Recent Advances and Prospects. *J. Mater. Chem. A* **2019**, *7*, 24150−24163.
(52) Wu, T.; Li, J.; Zou, Y.; Xu, H.; Wen, K.; Wan, S.; Bai, S.; Song, T.; McLeod, J. A.; Duhm, S.; Gao, F.; Sun, B. High-Performance Perovskite Light-Emitting Diode with Enhanced Operational Stability Using Lithium Halide Passivation. *Angew. Chem., Int. Ed.* **2020**, *59*, 4099−4105.
(53) Chen, X.; Zeng, J.; Kim, D.; Zheng, L.; Lou, Q.; Park, C. H.; Li, G. Understanding of Role of Li in High-Performance Pb-Free Li-Doped $(Ba_{0.85}Ca_{0.15})(Ti_{0.9}Zr_{0.1})O_3$ Piezoceramics from Theory and Experiments. *Mater. Chem. Phys.* **2019**, *231*, 173−180.
(54) Keshavarz, M.; Debroye, E.; Ottesen, M.; Martin, C.; Zhang, H.; Fron, E.; Küchler, R.; Steele, J. A.; Bremholm, M.; Van de Vondel, J.; Wang, H. I.; Bonn, M.; Roeffaers, M. B. J.; Wiedmann, S.; Hofkens, J. Tuning the Structural and Optoelectronic Properties of $Cs_2AgBiBr_6$ Double-Perovskite Single Crystals through Alkali-Metal Substitution. *Adv. Mater.* **2020**, *32*, No. 2001878.
(55) Zhao, W.; Yao, Z.; Yu, F.; Yang, D.; Liu, S. Alkali Metal Doping for Improved $CH_3NH_3PbI_3$ Perovskite Solar Cells. *Adv. Sci.* **2018**, *5*, No. 1700131.
(56) Li, Y.; Duan, J.; Yuan, H.; Zhao, Y.; He, B.; Tang, Q. Lattice Modulation of Alkali Metal Cations Doped $Cs_{1-x}R_xPbBr_3$ Halides for Inorganic Perovskite Solar Cells. *Sol. RRL* **2018**, *2*, No. 1800164.
(57) Kubicki, D. J.; Prochowicz, D.; Hofstetter, A.; Zakeeruddin, S. M.; Grätzel, M.; Emsley, L. Phase Segregation in Cs-, Rb- and K-Doped Mixed-Cation $(MA)_x(FA)_{1-x}PbI_3$ Hybrid Perovskites from Solid-State NMR. *J. Am. Chem. Soc.* **2017**, *139*, 14173−14180.
(58) Azmi, R.; Nurrosyid, N.; Lee, S.-H.; Al Mubarok, M.; Lee, W.; Hwang, S.; Yin, W.; Ahn, T. K.; Kim, T.-W.; Ryu, D. Y.; Do, Y. R.; Jang, S.-Y. Shallow and Deep Trap State Passivation for Low-Temperature Processed Perovskite Solar Cells. *ACS Energy Lett.* **2020**, *5*, 1396−1403.
(59) Kresse, G.; Hafner, J. Ab Initio Molecular Dynamics for Liquid Metals. *Phys. Rev. B* **1993**, *47*, No. 558.
(60) Jaeger, H. M.; Fischer, S.; Prezhdo, O. V. Decoherence-Induced Surface Hopping. *J. Chem. Phys.* **2012**, *137*, No. 22A545.
(61) Akimov, A. V.; Prezhdo, O. V. The PYXAID Program for Non-Adiabatic Molecular Dynamics in Condensed Matter Systems. *J. Chem. Theory Comput.* **2013**, *9*, 4959−4972.
(62) Akimov, A. V.; Prezhdo, O. V. Advanced Capabilities of the PYXAID Program: Integration Schemes, Decoherence Effects, Multiexcitonic States, and Field-Matter Interaction. *J. Chem. Theory Comput.* **2014**, *10*, 789−804.
(63) Li, L.; Long, R.; Bertolini, T.; Prezhdo, O. V. Sulfur Adatom and Vacancy Accelerate Charge Recombination in MoS_2 but by Different Mechanisms: Time-Domain Ab Initio Analysis. *Nano Lett.* **2017**, *17*, 7962−7967.
(64) Zhou, Z.; Liu, J.; Long, R.; Li, L.; Guo, L.; Prezhdo, O. V. Control of Charge Carriers Trapping and Relaxation in Hematite by Oxygen Vacancy Charge: Ab Initio Non-Adiabatic Molecular Dynamics. *J. Am. Chem. Soc.* **2017**, *139*, 6707−6717.
(65) Wang, L.; Long, R.; Prezhdo, O. V. Time-Domain Ab Initio Modeling of Photoinduced Dynamics at Nanoscale Interfaces. *Annu. Rev. Phys. Chem.* **2015**, *66*, 549−579.
(66) Chaban, V. V.; Prezhdo, V. V.; Prezhdo, O. V. Covalent Linking Greatly Enhances Photoinduced Electron Transfer in Fullerene-Quantum Dot Nanocomposites: Time-Domain Ab Initio Study. *J. Phys. Chem. Lett.* **2013**, *4*, 1−6.
(67) Li, L.; Long, R.; Prezhdo, O. V. Charge Separation and Recombination in Two-Dimensional MoS_2/WS_2: Time-Domain Ab Initio Modeling. *Chem. Mater.* **2017**, *29*, 2466−2473.
(68) Akimov, A. V.; Asahi, R.; Jinnouchi, R.; Prezhdo, O. V. What Makes the Photocatalytic CO_2 Reduction on N-Doped Ta_2O_5 Efficient: Insights from Nonadiabatic Molecular Dynamics. *J. Am. Chem. Soc.* **2015**, *137*, 11517−11525.
(69) Long, R.; Prezhdo, O. V. Asymmetry in the Electron and Hole Transfer at a Polymer−Carbon Nanotube Heterojunction. *Nano Lett.* **2014**, *14*, 3335−3341.
(70) Yang, Y.; Fang, W.-H.; Benderskii, A.; Long, R.; Prezhdo, O. V. Strain Controls Charge Carrier Lifetimes in Monolayer WSe_2: Ab Initio Time Domain Analysis. *J. Phys. Chem. Lett.* **2019**, *10*, 7732−7739.
(71) Lu, T.-F.; Wang, Y.-S.; Tomko, J. A.; Hopkins, P. E.; Zhang, H.-X.; Prezhdo, O. V. Control of Charge Carrier Dynamics in Plasmonic Au Films by TiO_x Substrate Stoichiometry. *J. Phys. Chem. Lett.* **2020**, *11*, 1419−1427.
(72) Li, W.; Chen, Z.; Tang, J.; Prezhdo, O. V. Anti-Correlation Between Band-Gap and Carrier Lifetime in Lead Halide Perovskites under Compression Rationalized by Ab Initio Quantum Dynamics. *Chem. Mater.* **2020**, *32*, 4707−4715.

https://dx.doi.org/10.1021/acs.chemmater.0c04188
Chem. Mater. 2021, 33, 1285−1292

(73) Wang, Y.; Long, R. Rapid Decoherence Induced by Light Expansion Suppresses Charge Recombination in Mixed Cation Perovskites: Time-Domain Ab Initio Analysis. *J. Phys. Chem. Lett.* **2020**, *11*, 1601−1608.
(74) Wang, J.; Li, W.; Yin, W. Passivating Detrimental DX Centers in $CH_3NH_3PbI_3$ for Reducing Nonradiative Recombination and Elongating Carrier Lifetime. *Adv. Mater.* **2019**, *32*, No. 1906115.
(75) Chu, W.; Zheng, Q.; Prezhdo, O. V.; Zhao, J.; Saidi, W. A. Low-Frequency Lattice Phonons in Halide Perovskites Explain High Defect Tolerance toward Electron-Hole Recombination. *Sci. Adv.* **2020**, *6*, No. eaaw7453.
(76) Ghosh, D.; Acharya, D.; Zhou, L.; Nie, W.; Prezhdo, O. V.; Tretiak, S.; Neukirch, A. J. Lattice Expansion in Hybrid Perovskites: Effect on Optoelectronic Properties and Charge Carrier Dynamics. *J. Phys. Chem. Lett.* **2019**, *10*, 5000−5007.
(77) He, J.; Casanova, D.; Fang, W.-H.; Long, R.; Prezhdo, O. V. MAI Termination Favors Efficient Hole Extraction and Slow Charge Recombination at $MAPbI_3$/CuSCN Heterojunction. *J. Phys. Chem. Lett.* **2020**, *11*, 4481−4489.
(78) Li, W.; Vasenko, A. S.; Tang, J.; Prezhdo, O. V. Anharmonicity Extends Carrier Lifetimes in Lead Halide Perovskites at Elevated Temperatures. *J. Phys. Chem. Lett.* **2019**, *10*, 6219−6226.
(79) Chu, W.; Saidi, W. A.; Zhao, J.; Prezhdo, O. V. Soft Lattice and Defect Covalency Rationalize Tolerance of B-$CsPbI_3$ Perovskite Solar Cells to Native Defects. *Angew. Chem., Int. Ed.* **2020**, *59*, 6435−6441.
(80) Li, W.; Long, R.; Tang, J.; Prezhdo, O. V. Influence of Defects on Excited State Dynamics in Lead Halide Perovskites: Time-Domain Ab Initio Studies. *J. Phys. Chem. Lett.* **2019**, *10*, 3788−3804.
(81) Li, W.; Tang, J.; Casanova, D.; Prezhdo, O. V. Time-Domain Ab Initio Analysis Rationalizes the Unusual Temperature Dependence of Charge Carrier Relaxation in Lead Halide Perovskite. *ACS Energy Lett.* **2018**, *3*, 2713−2720.
(82) Ghosh, D.; Neukirch, A. J.; Tretiak, S. Optoelectronic Properties of Two-Dimensional Bromide Perovskites: Influences of Spacer Cations. *J. Phys. Chem. Lett.* **2020**, *11*, 2955−2964.
(83) Li, W.; Liu, J.; Bai, F.-Q.; Zhang, H.-X.; Prezhdo, O. V. Hole Trapping by Iodine Interstitial Defects Decreases Free Carrier Losses in Perovskite Solar Cells: A Time-Domain Ab Initio Study. *ACS Energy Lett.* **2017**, *2*, 1270−1278.
(84) Liu, J.; Prezhdo, O. V. Chlorine Doping Reduces Electron−Hole Recombination in Lead Iodide Perovskites: Time-Domain Ab Initio Analysis. *J. Phys. Chem. Lett.* **2015**, *6*, 4463−4469.
(85) He, J.; Vasenko, A. S.; Long, R.; Prezhdo, O. V. Halide Composition Controls Electron−Hole Recombination in Cesium−Lead Halide Perovskite Quantum Dots: A Time Domain Ab Initio Study. *J. Phys. Chem. Lett.* **2018**, *9*, 1872−1879.
(86) Tong, C.-J.; Li, L.; Liu, L.-M.; Prezhdo, O. V. Synergy between Ion Migration and Charge Carrier Recombination in Metal-Halide Perovskites. *J. Am. Chem. Soc.* **2020**, *142*, 3060−3068.
(87) Baikie, T.; Fang, Y.; Kadro, J. M.; Schreyer, M.; Wei, F.; Mhaisalkar, S. G.; Graetzel, M.; White, T. J. Synthesis and Crystal Chemistry of the Hybrid Perovskite $(CH_3NH_3)PbI_3$ for Solid-State Sensitised Solar Cell Applications. *J. Mater. Chem. A* **2013**, *1*, 5628−5641.
(88) Even, J.; Pedesseau, L.; Jancu, J.-M.; Katan, C. Importance of Spin−Orbit Coupling in Hybrid Organic/Inorganic Perovskites for Photovoltaic Applications. *J. Phys. Chem. Lett.* **2013**, *4*, 2999−3005.
(89) Quarti, C.; Mosconi, E.; Umari, P.; De Angelis, F. Chlorine Incorporation in the $CH_3NH_3PbI_3$ Perovskite: Small Concentration, Big Effect. *Inorg. Chem.* **2017**, *56*, 74−83.
(90) Walsh, A. Principles of Chemical Bonding and Band Gap Engineering in Hybrid Organic-Inorganic Halide Perovskites. *J. Phys. Chem. C* **2015**, *119*, 5755−5760.
(91) Cohen, A. V.; Egger, D. A.; Rappe, A. M.; Kronik, L. Breakdown of the Static Picture of Defect Energetics in Halide Perovskites: The Case of the Br Vacancy in $CsPbBr_3$. *J. Phys. Chem. Lett.* **2019**, *10*, 4490−4498.
(92) Quarti, C.; Grancini, G.; Mosconi, E.; Bruno, P.; Ball, J. M.; Lee, M. M.; Snaith, H. J.; Petrozza, A.; De Angelis, F. The Raman Spectrum of the $CH_3NH_3PbI_3$ Hybrid Perovskite: Interplay of Theory and Experiment. *J. Phys. Chem. Lett.* **2014**, *5*, 279−284.
(93) Ma, J.; Wang, L.-W. Nanoscale Charge Localization Induced by Random Orientations of Organic Molecules in Hybrid Perovskite $CH_3NH_3PbI_3$. *Nano Lett.* **2015**, *15*, 248−253.
(94) Akimov, A. V.; Prezhdo, O. V. Persistent Electronic Coherence Despite Rapid Loss of Electron−Nuclear Correlation. *J. Phys. Chem. Lett.* **2013**, *4*, 3857−3864.
(95) Liu, J.; Kilina, S. V.; Tretiak, S.; Prezhdo, O. V. Ligands Slow Down Pure-Dephasing in Semiconductor Quantum Dots. *ACS Nano* **2015**, *9*, 9106−9116.
(96) Habenicht, B. F.; Kalugin, O. N.; Prezhdo, O. V. Ab Initio Study of Phonon-Induced Dephasing of Electronic Excitations in Narrow Graphene Nanoribbons. *Nano Lett.* **2008**, *8*, 2510−2516.
(97) Zhang, Z.; Fang, W.-H.; Tokina, M. V.; Long, R.; Prezhdo, O. V. Rapid Decoherence Suppresses Charge Recombination in Multi-Layer 2D Halide Perovskites: Time-Domain Ab Initio Analysis. *Nano Lett.* **2018**, *18*, 2459−2466.
(98) Palato, S.; Seiler, H.; Nijjar, P.; Prezhdo, O.; Kambhampati, P. Atomic Fluctuations in Electronic Materials Revealed by Dephasing. *Proc. Natl. Acad. Sci. U.S.A.* **2020**, *117*, 11940−11946.
(99) Kilina, S. V.; Neukirch, A. J.; Habenicht, B. F.; Kilin, D. S.; Prezhdo, O. V. Quantum Zeno Effect Rationalizes the Phonon Bottleneck in Semiconductor Quantum Dots. *Phys. Rev. Lett.* **2013**, *110*, No. 180404.

https://dx.doi.org/10.1021/acs.chemmater.0c04188
Chem. Mater. 2021, 33, 1285−1292